J Sol-Gel Sci Technol (2015) 76:260–270
DOI 10.1007/s10971-015-3773-6

ORIGINAL PAPER

Eu^{3+}-doped SiO_2–Gd_2O_3 prepared by the sol–gel process: structural and optical properties

Leonardo Alves Rocha[1] · Marco Antonio Schiavon[1] · Sidney José L. Ribeiro[2] · Rogéria Rocha Gonçalves[3] · Jefferson Luis Ferrari[1]

Received: 19 February 2015 / Accepted: 17 June 2015 / Published online: 28 June 2015

Abstract Eu^{3+}-doped SiO_2–Gd_2O_3 materials were prepared by the sol–gel process changing the Si^{4+}:Gd^{3+} molar ratio of 100:0, 70:30, 50:50, 30:70 and 0:100 mol%. The amount of Eu^{3+} was fixed at 0.2 mol% in relation to the total number of moles of [Si^{4+} + Gd^{3+}] in the systems. The xerogels obtained from sols were heat-treated at 900, 1000 and 1100 °C for 8 h. By TGA/DTA, XRD and Raman spectroscopy analysis, the formation of Gd_2O_3 crystalline was detected. The microstrains and crystallite size were calculated by the Williamson-Hall and Scherrer's equation, respectively. The results showed the direct dependence of microstrain and crystallite size as a function of the heat-treatment temperature. By the FTIR analysis was observed the elimination of species like H_2O, O–H and C–H groups, which can act as photoluminescence quenchers. All materials obtained in this work showed intense photoluminescence emission in the red region due to the $^5D_0 \rightarrow {}^7F_2$ transition of Eu^{3+}. The emission can be observed through the naked eye. The excited state lifetime shows to be dependent on values of refractive index and heat-treatment temperatures. The microstrain values affected the lifetime values and consequently the photoluminescence properties. In summary, the materials obtained in this work showed great absorption in the ultraviolet region promoting intense emission in the visible region, making them potential candidates for future applications in devices such as solar cells, image generator, biomarkers, among others.

Electronic supplementary material The online version of this article (doi:10.1007/s10971-015-3773-6) contains supplementary material, which is available to authorized users.

✉ Jefferson Luis Ferrari
jeffersonferrari@gmail.com; ferrari@ufsj.edu.br

[1] Grupo de Pesquisa em Química de Materiais (GPQM), Departamento de Ciências Naturais, Universidade Federal de São João del-Rei, Campus Dom Bosco, Praça Dom Helvécio, 74 – Fábricas, São João Del Rei, MG 36301-160, Brazil

[2] Instituto de Química, UNESP, P.O. Box 355, Araraquara, SP 14800-970, Brazil

[3] Departamento de Química, Faculdade de Filosofia, Ciências e Letras de Ribeirão Preto, USP, Av. Bandeirantes, 3900, Ribeirão Preto, SP 14040-901, Brazil

Graphical Abstract

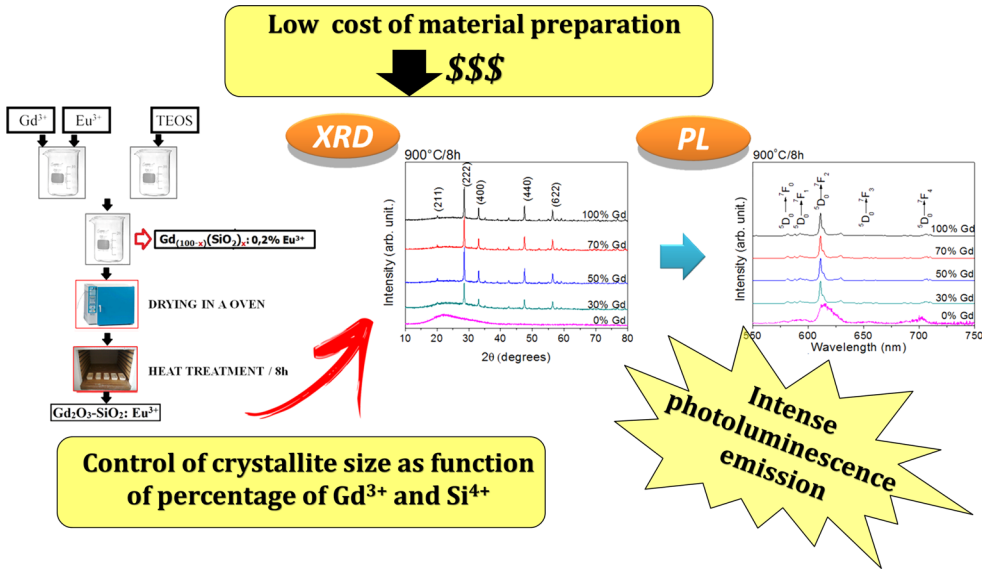

Keywords Photoluminescence · SiO_2–Gd_2O_3 · Sol–gel · Eu^{3+}-based phosphors

1 Introduction

Nowadays, there is a considerable growing quest for materials that present optical properties capable to contribute with the current demands of technological development [1]. In this sense, materials containing Rare Earth ions (RE^{3+}) have been one of the highlights in the development of new systems or even improving the properties of the existing ones. Among the RE^{3+}, different properties can be obtained due to different characteristics in the electronic configuration of these elements. When the RE^{3+} is embedded in the adequate host matrix, through doping process for instance [2], different properties like photoluminescence [3], magnetic [4], energy conversion [5], among others, can be obtained. The RE^{3+} has a low absorption coefficient assigned to the Laport rules, and when inserted in adequate matrix, the host can act as great sensitizer for these ions [6].

The Eu^{3+}, for instance, presents specific spectroscopic characteristics, which makes them an excellent ion for use in image generating devices, solid-state lasers, and moreover, its optical properties can be used as a structural probe. It is possible to excite the matrix in the ultraviolet region, and it transfers energy to the RE^{3+}, which emits light through intraconfigurational *f–f* transitions [7]. This property makes the materials containing RE^{3+} promising in the development of more efficient energy-conversion devices [5].

However, the photoluminescence phenomena of RE^{3+} are directly dependent on process that contributes to the excited states deactivation. The excited states responsible for photoluminescence can be deactivated by the presence of groups like as C–H, N–H and O–H [8], non-radiative process [9], among others.

The search of adequate host matrix for RE^{3+} has been extensively discussed and reported in the literature. The search for an effective methodology to incorporate these ions in matrix is essential for the development of efficient photoluminescent systems. Many routes have been reported in different works in literature about the versatile and good way to prepare RE^{3+}-doped materials. Among them are solid-state synthesis [10], combustion method [11], co-precipitation method [12], sol–gel process [13], and others.

The sol–gel process is very interesting because it allows to control the molar ratio as well as the chemical composition of precursors. Consequently, the sol–gel process allows to control the refractive index of materials [9], and enables to increase the solubility of the ions in the host matrix [14, 15].

In literature, there are many works reporting about binary systems based on RE^{3+}-doped metal oxide–SiO_2 obtained by sol–gel process with excellent optical and structural properties very well discussed. Among some works, it is possible to cite SiO_2–ZrO_2 [16], Ta_2O_5–SiO_2 [9], HfO_2–SiO_2 [17] and SiO_2–TiO_2 [18] used as a host for RE^{3+}. These studies have also shown the influence and properties of RE^{3+}-doped metal oxide embedded in the silica amorphous phase as matrix.

In this work, the choice of the Gd_2O_3 as host matrix for Eu^{3+} is due to the fact that this oxide has a low phonon energy of lattice, around 600 cm^{-1} [19], good chemical

stability, and high thermal stability, allowing it to be processed with high temperature of synthesis [20]. Additionally, a few studies reports the use of Gd_2O_3–SiO_2 binary system as a host for RE^{3+} [21, 22], but still it is necessary to understand with more detail as the ratio between SiO_2 and Gd_2O_3 affect the photoluminescence of RE^{3+}, and as the sol–gel process allows to control with accuracy the composition of the materials.

In this sense, the aim of this work is to obtain and optimize the system Gd_2O_3–SiO_2 as host matrix for Eu^{3+} obtained by the sol–gel process. The changing of molar ratio between Si^{4+} and Gd^{3+} in the matrix composition, heat-treatment temperature, studying the optical and structural properties, comparing the behavior of materials based on Eu^{3+}-doped Gd_2O_3 and Eu^{3+}-doped SiO_2 are the main focus and challenge of this work.

2 Materials and methods

The experimental procedure used in this work was based on the same way reported by Ferrari et al. [9]. TEOS (Tetraethoxysilane—Sigma Aldrich—98 %) was used as precursor, and the oxides Eu_2O_3 (Europium oxide—Sigma Aldrich—99.99 %) and Gd_2O_3 (Gadolinium oxide—Sigma Aldrich—99.99 %) were dissolved in hydrochloric acid, and then, the solvent exchange was performed by anhydrous ethanol, obtaining individual alcoholic solutions of Eu^{3+} and Gd^{3+} with concentrations of 0.1 mol L^{-1}. These solutions were standardized via complexometric titration using EDTA 0.01 mol L^{-1}. To obtain the Eu^{3+}-doped SiO_2–Gd_2O_3-based materials, the various Si^{4+}/Gd^{3+} ratios were 100:0, 70:30, 50:50, 30:70 and 0:100 mol%, respectively. The systems were doped with 0.2 mol% of Eu^{3+} in relation to the total number of moles of [Gd^{3+} + Si^{4+}]. The corresponding amount of TEOS was added into a beaker, and HCl was added with 50:1 ratio TEOS/HCl, and the total volume was diluted to 10 mL with anhydrous ethanol P.A. In the second beaker, the exact volume of anhydrous ethanol solution containing Gd^{3+} and the exact volume of solution containing Eu^{3+} were added, and finally, the volume was diluted to 10 mL with anhydrous ethanol, under constant stirring. Both solutions were stirred for 15 min. Then, the TEOS solution was added to the metal solution, and constantly stirred for 15 min to homogenize the solution to obtain the sol. Then, the sols obtained containing different relationships between Si^{4+} and Gd^{3+} were kept in an oven of approximately 100 °C for 24 h to obtain the xerogel, which was crushed in an agate mortar and submitted to heat treatment at 900, 1000 and 1100 °C for 8 h.

The thermal stability of xerogels obtained were analyzed from room temperature up to 1000 °C operating a Thermogravimetric and Differential Thermal Analyzer (TGA/DTA; DTG-60H, Shimadzu, Maryland, USA) under synthetic air atmosphere, and a heating rate of 10 °C/min. The powders crystalline structures were characterized by X-ray diffraction spectroscopy (XRD) using the diffractometer model XRD 6000, Shimadzu, using Cu $K_\alpha = 1.5418$ Å radiation, graphite monochromator, step of 0.02° degrees with 2θ region between 10° and 80°. Based on the diffraction patterns obtained, the crystallite sizes were calculated using Scherrer's equation. The materials were also characterized by Raman spectroscopy using a Raman spectrometer (LabRAM HR, Horiba Jobin–Yvon Inc., New Jersey, USA) with laser as excitation source at 632.8 nm. The materials obtained were also characterized by Fourier transform infrared spectroscopy (FTIR) to verify the presence of possible photoluminescence deactivator groups. The samples were macerate in an agate mortar with 100 mg of KBr. and were kept under pressure of 10 tons for 1 min, obtaining the pastilles. The FTIR spectra were obtained in the region between 4000 and 400 cm^{-1} operating a Fourier transformed IR spectrometer (FTIR; Perkin Elmer, Spectrum GX, Wellesley, MA) in transmission mode with resolution of 4 cm^{-1}. The shape of materials was evaluated by scanning electron microscopy (SEM; Hitachi TM3000, Hitachi High-Technologies Co., Ltd., Tokyo, Japan) with energy dispersive X-ray diffraction spectroscopy (EDX; Bruker, Quantax 70, Berlin, Germany). The materials obtained after thermal treatments at

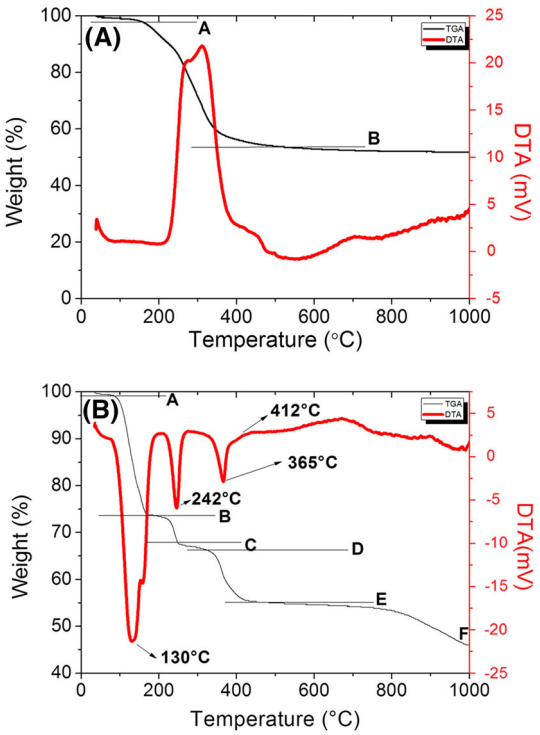

Fig. 1 TGA/DTA analysis of Eu^{3+}-doped xerogels with composition: **a** 100 mol% of Si^{4+} and **b** 100 mol% of Gd^{3+}

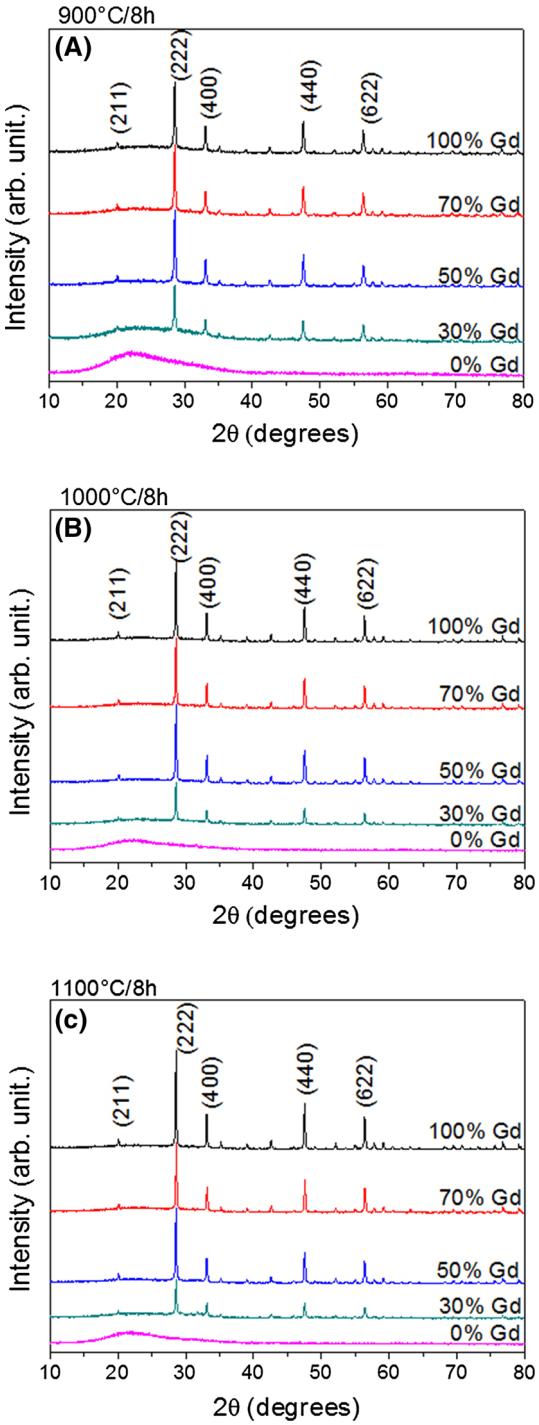

Fig. 2 Diffractograms obtained of Eu^{3+}-doped materials heat-treated at: **a** 900, **b** 1000 and **c** 1100 °C for 8 h

different temperatures were submitted to photoluminescence spectroscopy. The emission spectra were collected operating a (Horiba–Jobin–Yvon Fluorolog 3, Horiba Scientific, New Jersey, USA) with excitation source at 255 nm using a Xe lamp of 450 W. The photomultiplier was used as detector. The emission spectra were collected at room temperature in the region between 550 and 750 nm with excitation and emission slits of 5 and 1 nm, respectively, using filter cutoff below 399 nm. The photoluminescence of the signals was measured at an angle of 22.5° in relation to the excitation source. The excitation spectra were obtained at room temperature in the region between 200 and 550 nm with excitation and emission slits of 5 and 1 nm, respectively, fixing the wavelength of emission at 612 nm. The lifetime $^5D_0$ of Eu^{3+} was achieved using a pulsed lamp fixing device having excitation and emission at 255 and 612 nm, respectively, and all curves were obtained at room temperature.

3 Results and discussion

By TGA/DTA analysis, the steps of all reactions by which xerogels were obtained by the sol–gel process were investigated, and the loss of mass of final product was determined. Based on Fig. 1a, it can be seen that the system containing only silicon depicts one single-step and exothermic event around 310 °C, attributed to the decomposition of organic matter from TEOS used as precursor. Only at 500 °C, all the water and organic matter were removed. In Fig. 1b, it is shown that, the composition containing only Gd^{3+}, approximately 54 % of the mass was lost. During the materials formation, three endothermic steps are observed in DTA analysis: first at 130 °C (A–B), which corresponds to the elimination of all water remaining, a second step between 242 °C (B–C) and 365 °C (C–D) is assigned to the elimination of organic matter and as third step around 412 °C, the crystallization of Gd_2O_3 phase [23] occurs, and after 800 °C (E–F) no other change related to the loss of mass it is observed.

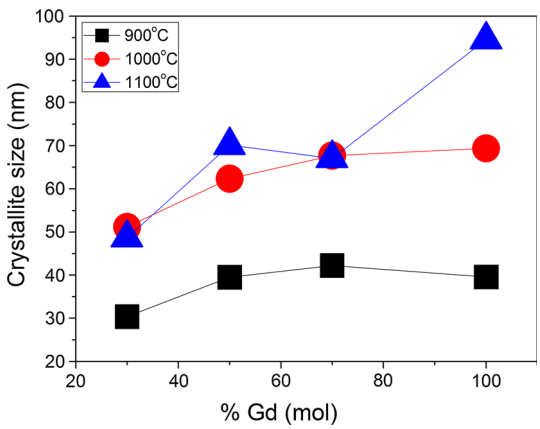

Fig. 3 Crystallite sizes obtained by Scherrer's equation as a function of the Gd^{3+} concentration and at different heat-treatment temperatures

XRD analysis allowed to evaluate the materials crystallinity and the phases formed at 900, 1000 and 1100 °C. Fig. 2 demonstrates that in all materials containing Gd^{3+}, the diffraction patterns showed intense reflections attributed to the crystalline phase of cubic type with lattice parameters $a = b = c = 10.813$ Å, and $\alpha = \beta = \gamma = 90°$, according to the data in JCPDF cards $n° = 00–012–0797$. The reflection peaks observed in the diffraction pattern were attributed to the crystallographic *hkl* planes: (211), (222) (400) (440) and (622) localized at $2\theta = 20.07°$, 28.58°, 33.12°, 47.52° and 56.40°, respectively. Increasing the Gd^{3+} concentration, as well as increasing the heat-treatment temperature, an increase in intensity of the reflections is observed. This effect can be associated with the increasing of the crystalline portion of Gd_2O_3 phase in the system.

In materials obtained from the xerogel prepared only from TEOS used as precursor, it was observed that after heat treatment occurs the formation of amorphous phase assigned to the SiO_2. This affirmation is due to the presence of a broad peak in the diffractogram, located in the region between 15° and 25° with maximum around 21°, characteristic of an amorphous SiO_2 system.

Using the Scherrer's equation (Eq. 1), it was possible to calculate the crystallite size, based on reflection peak attributed to the *hkl* plane (222) positioned at $2\theta = 28.56°$. In the Scherrer's equation, D is the size of crystallite, K is the shape factor (in this work was used 0.89), λ is the wavelength of X-rays (CuKα = 1.5418 Å) and β_{hkl} the full width of the half maximum (FWHM) of the most intense peak. The β values were adjusted according to Eq. 2, where β_{inst} is the FWHM of the peak of standard that is related to the instrumental analysis and β_{exp} is the FWHM of most intense peak of the sample was experimentally analyzed. The standard used in this work was the Si (100) monocrystal.

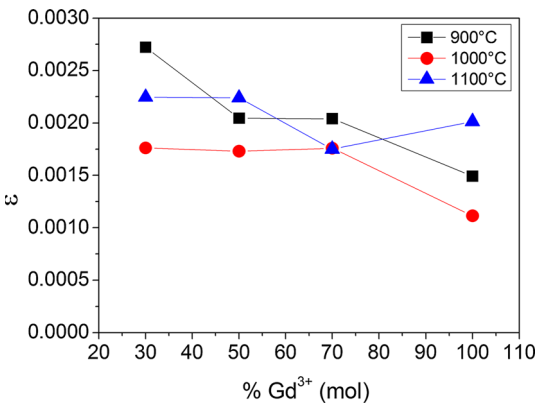

Fig. 4 Microstrain values as a function of Gd^{3+} concentration and different heat-treatment temperatures, determined by W–H methods

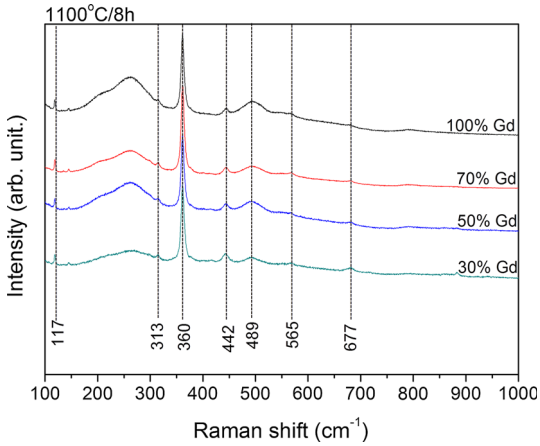

Fig. 5 Raman Spectra of Eu^{3+}-doped Gd_2O_3-based materials heat-treated at 1100 °C for 8 h

$$D_{hkl} = \frac{K \cdot \lambda}{\beta_{hkl} \cos\theta} \quad (1)$$

$$\beta_{hkl} = \sqrt{\beta^2{}_{\exp} - \beta^2{}_{inst}} \quad (2)$$

The results obtained are shown in Fig. 3. It was observed that there is an increase in crystallite size as a function of heat-treatment temperature. This behavior is due to the coalescence/aggregation of Gd_2O_3 crystals by the higher thermal energy applied on system, thereby reducing the surface free energy, and providing greater driving force for the growth of crystals [24]. Moreover, it was observed that increasing the Gd^{3+} amount favors an increase in crystallite size. This behavior can be explained by the fact that the larger amounts of Gd^{3+} are available favoring the increase in crystals size.

Through the Williamson-Hall method (W–H), also called Uniform Deformation Model (UDM), according to the Eq. 3, the microstrain values were calculated [25, 26]. The method is also recently reported for analyzing the behavior of the particle size of ZnO [26] and can be applied to understand the behavior of other kind of systems, like the Gd_2O_3. The microstrain values obtained in this work are shown in Fig. 4.

$$\beta_{hkl} \cos\theta = \frac{K \cdot \lambda}{D} + 4\varepsilon \sin\theta \quad (3)$$

In Fig. 4, it is observed that the increase in Gd^{3+} concentration in the system promotes the reduction in microstrain values. Also it is noted that samples heat-treated at 1000 °C show lower microstrain values. Therefore, the decrease in microstrain values as a function of the heat-treatment temperature is observed, due to the closing of the pores and the reduction of defects in heat-treatment process.

The samples heat-treated at 1100 °C that presented larger crystals were submitted to Raman spectroscopy, and

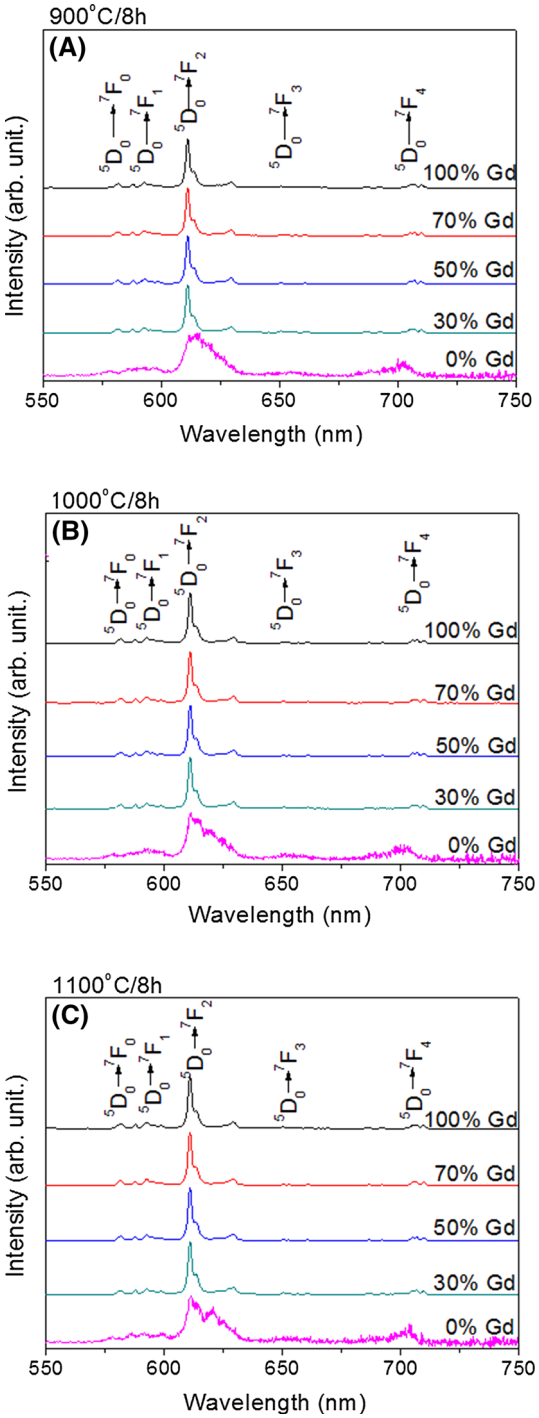

Fig. 6 Photoluminescence emission spectra under excitation at 255 nm of Eu^{3+}-doped materials heat-treated at **a** 900, **b** 1000 e **c** 1100 °C for 8 h

the spectra are shown in Fig. 5. The spectra shows the most intense band localized around 360 cm^{-1}, assigned to the mode $E_g + F_g$, associated with the Gd_2O_3 cubic phase with space group *Ia-3* (206) [27]. The results are in agreement with the XRD analysis. Bands positioned around 117, 313, 442, 565 and 677 cm^{-1} are also associated with the Gd_2O_3 cubic phase, compatible to commercial oxide [28]. All samples containing Gd^{3+} showed a band around 489 cm^{-1}, attributed to the A_g mode, characteristic of the hexagonal phase of Gd_2O_3 [29]. To obtain the cubic phase, during the heat-treatment, the gadolinium oxide is formed in the hexagonal structure at lower temperatures, and then, increasing the temperature of heat-treatment, the cubic phase is obtained. In this sense, this single band can be associated with the presence of little amount hexagonal phase remaining in the sample, undetected by the XRD analysis.

In Fig. 6 are shown the emission spectra obtained of the samples heat-treated at 900, 1000 and 1100 °C. In all spectra obtained were observed bands assigned to the intraconfigurational *f–f* transition of Eu^{3+} from $^5D_0$ to ^7F_J energy levels, where $J = 0$, 1, 2, 3 and 4 [7]. The Eu^{3+}-doped Gd_2O_3-based materials showed thinner and well-defined photoluminescent emissions bands. The Gd^{3+} absorbs energy in the UV region and transfer to Eu^{3+} efficiently [30], resulting an intense emission band. In the Eu^{3+}-doped Gd_2O_3 cubic structure, the Eu^{3+} can occupy two different sites of symmetry, in which the probability of occupation is around 25 % of ions in S_6 site (with inversion center) and 75 % in C_2 site (without inversion center) [31].

The Eu^{3+} shows a strong emission band in the red region positioned around 612 nm, attributed to the $^5D_0 \rightarrow {}^7F_2$ energy level. This emission, electric-dipole-allowed, known as hypersensitive, occurs when the Eu^{3+} is positioned in site of symmetry with absence of inversion center [7, 32]. The intensity of $^5D_0 \rightarrow {}^7F_1$ transition, (allowed by magnetic dipole), is not affected by the local symmetry being independent where the Eu^{3+} is located in the host matrix [3, 33]. The ratio between the integrated areas of $^5D_0 \rightarrow {}^7F_2$ (allowed by electric dipole) and $^5D_0 \rightarrow {}^7F_1$ (allowed by magnetic dipole) transitions were calculated and labeled as R_{21}. As the intensity of the $^5D_0 \rightarrow {}^7F_1$ transition is not affected by the chemical environment in which the Eu^{3+} is located and the transition $^5D_0 \rightarrow {}^7F_2$ is very sensitive to this environment, the ratio between the areas of both transitions allows to investigate the Eu^{3+} position in the matrix. The results for R_{21} are shown in Table 1. Increasing the heat-treatment temperature and concentration of Gd^{3+} in the binary system, the R_{21} value decreases. This means that the increasing the heat-treatment temperature and the percentage of Gd^{3+}, the Eu^{3+} occupies sites with high symmetry, decreasing the probability of the $^5D_0 \rightarrow {}^7F_2$ transition to occur. This ratio also can be used to compare the photoluminescence intensities of materials in powder forms. The highest R_{21} values for the materials obtained in this work indicate that the Eu^{3+} predominantly occupies sites with lower symmetry or some sites with high symmetry slightly distorted,

Table 1 R_{21} values for materials obtained at 900, 1000 e 1100 °C doped with 0.2 mol% of Eu^{3+}

Sample—ratio between Si^{4+}:Gd^{3+} (mol%)	Temperature (°C)	R_{21}
0:100	900	4.01
30:70		4.00
50:50		4.13
70:30		4.46
100:0		5.02
0:100	1000	3.85
30:70		3.81
50:50		3.92
70:30		3.82
100:0		4.58
0:100	1100	3.77
30:70		3.77
50:50		3.87
70:30		3.87
100:0		4.69

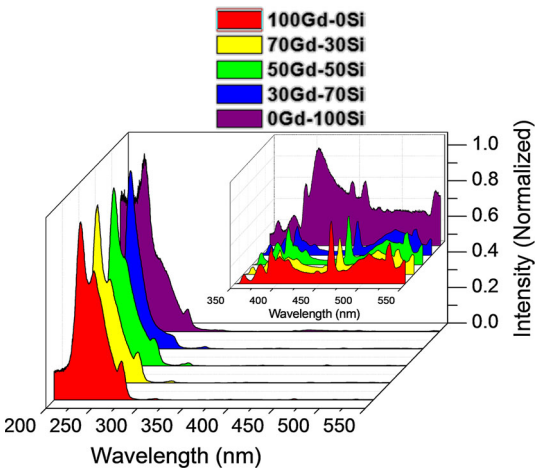

Fig. 7 Photoluminescence excitation spectra with emission fixed at 612 nm of Eu^{3+}-doped materials heat-treated at 900 °C for 8 h

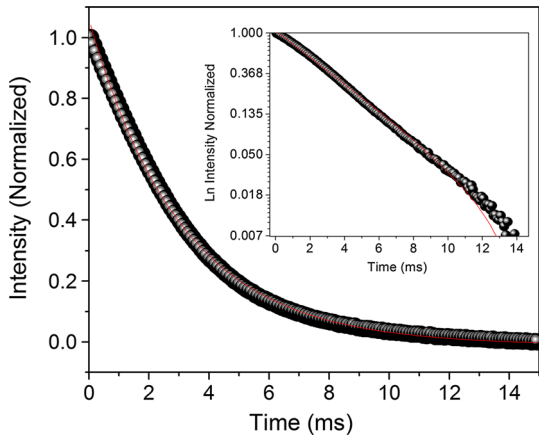

Fig. 8 Emission–decay curve of the Eu^{3+}-doped material with molar ratio of $70Si^{4+}$:$30Gd^{3+}$ heat-treated at 900 °C for 8 h with emission and excitation fixed at 612 and 255 nm, respectively

Table 2 Refractive index values calculated by Lorentz–Lorenz's equation

Gd^{3+} (mol%)	Si^{4+} (mol%)	Refractive index value
100	0	1.80 [35]
70	30	1.66
50	50	1.61
30	70	1.55
0	100	1.45 [35]

promoting higher photoluminescence intensity. The Eu^{3+}-doped SiO_2 presents high R_{21} values, but its photoluminescence intensity assigned to the $^5D_0 \rightarrow {}^7F_2$ is hundred times lesser than the materials containing Gd^{3+}. All Eu^{3+}-doped compositions without Gd^{3+}, containing only Si^{4+} precursors, showed a large emission bands and low photoluminescence intensity in the red region. The broadening of the most intense band in the emission spectra is characteristic of Eu^{3+} situated in amorphous systems. These bands with inhomogeneous broadening are indicative of Eu^{3+} positioned in different sites of silica host [34]. As observed by XRD, the silica network presents an amorphous system, without structural periodicity, in which characterizes the enlargement profile of emission bands of Eu^{3+} present in these kinds of materials [33].

The lowest photoluminescence intensity of the samples based on Eu^{3+}-doped SiO_2 can be attributed to the lowest absorption of UV radiation of SiO_2. In the Fig. 7 are shown the excitation spectra of all materials heat-treated at 900 °C, with emission fixed at 612 nm. The SiO_2-based materials present low absorption at short

Table 3 Lifetime values of all Eu^{3+}-doped samples with emission and excitation fixed at 612 and 255 nm, respectively

Samples ratio between Si^{4+}:Gd^{3+} (mol%)	Temperature (°C)	Lifetime (ms)
0:100	900	2.67
	1000	2.69
	1100	2.38
30:70	900	2.83
	1000	3.05
	1100	2.49
50:50	900	3.17
	1000	3.14
	1100	2.79
70:30	900	3.10
	1000	3.23
	1100	3.06
100:0	900	1.77
	1000	1.87
	1100	1.30

wavelengths, resulting in low efficiency of energy transfer to Eu^{3+}. The lower efficiency in the energy transfer also can be related to the presence of defects in the structure of SiO_2.

The refractive index of the binary systems, n, was calculated by the Lorentz–Lorenz Equation (Eq. 4), where n_a is the Gd_2O_3 refractive index, n_b the SiO_2 refractive index, f_a is the Gd_2O_3 molar fraction and f_b the SiO_2 molar fraction. The Gd_2O_3 and SiO_2 refractive index used were 1.8 and 1.45 (at 633 nm), [35] respectively. Comparison of the final concentrations of each metal in the samples was determined by the EDX analysis. The refractive index values are shown in Table 2. The increasing of SiO_2 concentration promotes the decreasing of refractive index of the materials.

$$\frac{n^2-1}{n^2+2} = f_a \frac{(n_a^2-1)}{(n_a^2+2)} + f_b \frac{(n_b^2-1)}{(n_b^2+2)} \tag{4}$$

The lifetime values of $^5D_0$ state of Eu^{3+} were obtained under excitation and emission fixed at 255 and 612 nm, respectively. The lifetime values were calculated, and in Fig. 8, the decay curve of the system containing 30 mol% of Gd^{3+} heat-treated at 900 °C is shown. The profile of curve is representative for all materials obtained in this work, and adjusted on the first-order exponential decay, with a correlation coefficient $R \cong 1$. The values obtained are presented in Table 3.

The radiative lifetime can be related to the refractive index of the medium [36], and an electronic dipole transition may be expressed by the Eq. 5. In Eq. 5, the $\hbar$ is h/2π, e is charge of the electron, m is the mass of the electron, ω_{if} is the frequency, μ_{if} is the dipole moment of the transition, λ_0 is the wavelength of the emission in vacuum and n is the refractive index of the material in the wavelength of emission [37, 38].

$$t_R \approx \frac{3\hbar e^2}{2m\omega_{if}|\mu_{if}|^2} \frac{\lambda_0^2}{\left[\frac{1}{3}(n^2+2)\right]^2 n} \tag{5}$$

According to the Eq. 5, the radiative lifetime is inversely proportional to the refractive index [37, 38]. On this way, as calculated by Lorentz–Lorenz methods, the binary system presents lower refractive index in comparison to the system containing only Gd_2O_3, which promotes the increase in the radiative lifetime. Table 3 presents the lifetime values of materials obtained in this work. For the 70:30, 50:50 and 30:70, the SiO_2 can be acting as shell of Gd_2O_3, and consequently contributing to the elimination of surface defects on the Gd_2O_3 particles, decreasing the non-radiative process, increasing the values of total lifetime.

The samples heat-treated at 1000 °C show higher lifetime values in most of compositions. The reduction of microstrain values in the crystal lattice were observed by the W–H calculus. Then, probably the decrease in defects in the structure can contribute to the elimination of non-radiative process, and consequently contributing to the higher lifetime values of the excited state of the Eu^{3+}.

The Eu^{3+}-doped SiO_2 systems have lifetime values between 1.30 and 1.87 ms, in which are the lowest values in comparison with the other materials reported here. This behavior can be associated with the presence of defects in the SiO_2 systems, as reported previously. The samples based only Eu^{3+}-doped Gd_2O_3 showed lifetime values between 2.38 and 2.67 ms.

Theses lifetime values can be related to the high chemical compatibility between Eu^{3+} and Gd^{3+} present in the host matrix. The difference of ionic radii between Gd^{3+}

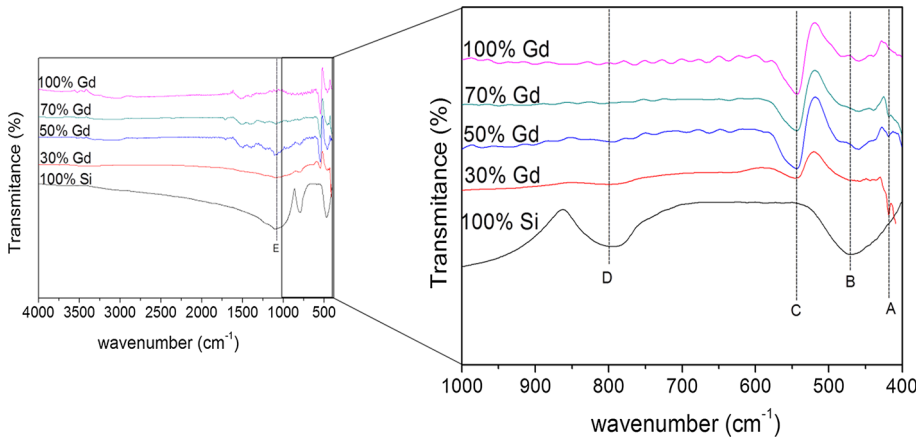

Fig. 9 FTIR spectra obtained for the materials heat-treated at 900 °C for 8 h

(1.078 Å) and Eu^{3+} (1.087 Å) [39] is very small, in which favors the almost perfect accommodation of the Eu^{3+} in Gd_2O_3. Consequently, this characteristic promotes adequate distance between Eu^{3+} in the structure, preventing a pronounced effect of cross-relaxation process.

In Fig. 9 are shown FTIR spectra of compositions containing 0.2 mol% of Eu^{3+} heat-treated at 900 °C. For better visualization the bands in the spectra, the region between 400 and 1000 cm^{-1} was amplified, and the bands assignments based on works reported in literature [3, 35, 40–42]. The A and C-band, located at 410 and 540 cm^{-1}, respectively, are attributed to the stretching of the Gd-O chemical bonding [3]. These bands are evident as a function of Gd^{3+} concentration, and absent in the spectra of the system containing only SiO_2. The band positioned approximately 470 cm^{-1} (B-band) is assigned to the Si–O–Si angular deformation [35]. The band positioned around 800 cm^{-1} (D-band) is attributed to the Si–O–Si stretching, and the band at approximately 1079 cm^{-1} (E-band) attributed to the Si–O–Si asymmetrical stretching. The appearance of these bands in the spectra is an evidence of formation of SiO_2 network [40–42]. The I-band located around 3400 cm^{-1} is attributed to the stretching of the O–H groups, and the intensity of this band decreases as a function heat-treatment temperature. In this sense, the temperature of heat-treatment contributed significantly to the elimination of the species, like O–H, C–H and N–H groups.

4 Conclusions

Eu^{3+}-doped SiO_2–Gd_2O_3 materials were obtained by the sol–gel process with success, and obtained very easily. In all materials obtained was observed an intense photoluminescence emission in the red region of the electromagnetic spectrum, attributed to the $^5D_0 \rightarrow {}^7F_2$ transition of Eu^{3+}. The crystallinity of the system was affected by the heat-treatment temperature, influencing directly on crystallite size and microstrain values, as observed by the Scherrer's and Williamson-Hall calculus, respectively. The crystallite size and microstrain also affected the photoluminescent properties of the materials reported. Controlling the heat-treatment temperature was possible to control the elimination of groups like as O–H and C–H, minimizing losses via non-radiative processes. Thus, it was observed that the materials heat-treated at 1000 °C showed better photoluminescent properties and lower microstrain values in comparison with the other material obtained. In summary it was possible to optimize the matrix based on SiO_2–Gd_2O_3, and verify that the binary system favors the emission of Eu^{3+}, presenting better results than Eu^{3+}-doped SiO_2 or Eu^{3+}-doped Gd_2O_3. The composition containing 70 and 30 mol% of Si^{4+} and Gd^{3+}, respectively, showed better performance as host matrix for RE^{3+} and lower cost of preparation. The materials obtained in this work showed potential properties for many applications in photonics areas and energy conversion, like solar cells.

Acknowledgments The authors gratefully acknowledge to Fundação de Amparo à Pesquisa do Estado de Minas Gerais (FAPEMIG) and Conselho Nacional de Desenvolvimento Científico e Tecnológico (CNPq), Fundação de Amparo à Pesquisa do Estado de São Paulo (FAPESP), Coordenação de Aperfeiçoamento de Pessoal de Nível Superior (CAPES). This work is a collaboration research project of members of the Rede Mineira de Química (RQ-MG) supported by FAPEMIG (Project: REDE-113/10). The authors also acknowledge Mr. Emílio Dias Moreira for SEM images. J.L. Ferrari also thanks Jenifer Esbenshade for English revisions.

References

1. Blasse G, Grabmaier BC (1994) Luminescent materials. Springer, Berlin

2. Gregorkiewicz T, Thao DTX, Langer JM (1998) Role of shallow bound states in emission processes of rare-earth doped semiconductors. Phys State Sol B 210:737–745
3. Dhananjaya N, Nagabhushana H, Nagabhushana BM, Rudraswamy B, Shivakumara C, Chakradhar RPS (2012) Spherical and rod-like Gd_2O_3:Eu^{3+} nanophosphors—structural and luminescent properties. Bull Mater Sci 35:519–527
4. Adkari AB, Shinde TJ, Vasambekar PN (2010) Magnetic properties of rare earth ion (Sm^{3+}) added nanocrystalline Mg–Cd ferrites, prepared by oxalate co-precipitation method. J Magn Magn Mater 322:3823–3827
5. Wild J, Meijerink A, Rath JK, Van Sark WGJHM, Schropp REI (2011) Upconverter solar cells: materials and applications. Energy Environ Sci 4:4835–4848
6. Polman A, van Veggel FCJM (2004) Broadband sensitizers for erbium-doped planar optical amplifiers: review. J Opt Soc Am B 21:871–892
7. Malta OL (1982) Theoretical crystal-field parameters for the YOC1-Eu^{3+} system: a simple overlap model. Chem Phys Lett 88:353–356
8. Moon T, Hwang S, Jung D, Son D, Kim C, Kim J, Kang M, Park B (2007) Hydroxyl-Quenching effects on the photoluminescence properties of SnO_2:Eu^{3+} nanoparticles. J Phys Chem C 111:4164–4167
9. Ferrari JL, Lima KO, Pecoraro E, Gonçalves RR, Ferreira R, Carlos LAD (2012) Color tunability of intense upconversion emission from Er^{3+}/Yb^{3+} co-doped SiO_2–Ta_2O_5 glass ceramic planar waveguides. J Mater Chem 22:9901–9908
10. Wang W, Zhang X, Haotian J, Dong T, Yang D (2012) Fabrication of Er^{3+}/Yb^{3+} co-doped Y_2O_3 transparent ceramics by solid-state reaction method and its up-conversion luminescence. Mater Chem Phys 135:709–713
11. Dhananjayaa N, Nagabhushanac H, Nagabhushanad BM, Rudraswamya B, Shivakumarae C, Chakradhar RPS (2011) Effect of Li^{+}-ion on enhancement of photoluminescence in Gd_2O_3:Eu^{3+} nanophosphors prepared by combustion technique. J Alloys Compd 509:2368–2374
12. Szczeszak A, Lis S, Nagirnyi V (2011) Spectroscopic properties of Eu^{3+} doped YBO_3 nanophosphors synthesized by modified co-precipitation method. J Rare Earths 29:1142–1146
13. Chiasera A, Montagna M, Rolli R, Ronchin S, Pelli S, Righini GC, Gonçalves RR, Messadeq Y, Ribeiro SJL, Armelini C, Ferrari M, Zampedri L (2003) Er^{3+}/Yb^{3+} co-activated sílica-alumina monolithic xerogels. J Sol-Gel Sci Technol 26:943–946
14. Livage J, Henry M, Sanchez C (1988) Sol–gel chemistry of transition metal oxides. Prog Solid State Chem 18:250–341
15. Yamane M, Asahara Y (2000) Glass for photonics. Cambridge University Press, Cambridge
16. Gonçalves RR, Guimaraes JJ, Ferrari JL, Maia LJQ, Ribeiro SJL (2008) Active planar waveguides based on sol gel Er^{3+}-doped SiO_2 ZrO_2 for photonic applications: morphological, structural and optical properties. J Non-cryst Solid 354:4846–4851
17. Zampedri L, Righini GC, Portales H, Pelli S, Nunzi Conti G, Montagna M, Mattarelli M, Gonçalves RR, Ferrari M, Chiasera A, Bouazaoui M, Armellini C (2004) Sol–gel derived Er-activated SiO_2–HfO_2 planar waveguides for 1.5 μm application. J Non-cryst Solid 345:580–584
18. Castañeda-Contreras J, Meneses-Nava MA, Barbosa-García O, Rodríguez-Rojas RA, Félix MV (2006) Visible erbium luminescence in SiO_2–TiO_2–Er^{3+} sol–gel powders. Opt Mater 29:38–42
19. Guo H, Dong N, Yinm M, Lou L, Xia S (2004) Visible upconversion in rare earth ion-doped Gd_2O_3 nanocrystals. J Phys Chem B 108:19205–19209
20. Ferrari JL, Parreira RLT, Pires AM, Lima SAM, Davolos MR (2011) A route to obtain Gd_2O_3:Nd^{3+} with different particle size. Mater Chem Phys 127:40–44
21. Liu G, Hong G, Sun D (2004) Synthesis and characterization of SiO2, Gd2O3: Eu core–shell luminescent materials. J Colloid Interface Sci 278:133–138
22. Dramicanin MD, Jokanovic V, Andric Z, Viana B, Aschehoug P, Antic-Fidancev E (2006) Synthesis, structural and luminescent properties of Gd_2O_3–SiO_2:Eu^{3+} nanopowder composites. Mater Sci Forum 518:455–458
23. de Ramírez AJM, Murillo AG, de Romo FJC, Hernández MG, Vigueras DJ, Chaderyron G, Boyer D (2010) Properties of Gd_2O_3:Eu^{3+}, Tb^{3+} nanopowders obtained by sol–gel process. Mater Res Bull 45:40–45
24. Burda C, Chen X, Nrayanan R, El-Sayed MA (2005) Chemistry and properties of nanocrystals of different shapes. Chem Rev 105:1025–1102
25. Williamson GK, Hall WH (1953) X-ray line broadening from filed aluminium and wolfram. Acta Metall 1:22–31
26. Mote VD, Purushotham Y, Dole BN (2012) Willianson-Hall analysis in estimations of lattice strain in nanometer-sized ZnO particles. J Theor Appl Phys 6:1–8
27. Rajan G, Gopchandran KG (2009) Enhanced luminescence from spontaneously ordered Gd_2O_3:Eu^{3+} based nanostructures. Appl Surf Sci 255:9112–9123
28. García-Murillo A, Le Luyer A, Dujardin C, Pedrini C, Mugnier J (2001) Elaboration and characterization of Gd_2O_3 waveguiding thin films prepared by the sol–gel process. Opt Mater 16:39–46
29. Dhananjaya N, Nagabhushana H, Nagabhushana BM, Rudraswamy B, Shivakumara C, Chakradhar RPS (2011) Hydrothermal synthesis, characterization and Raman studies of Eu^{3+} activated Gd_2O_3 nanorods. Phys B 406:1639–1644
30. Hachani S, Moine B, Al-Akrmi A, Férid M (2009) Luminescent properties of some ortho- and pentaphosphates doped with Gd^{3+}–Eu^{3+}: potential phosphors for vacuum ultraviolet excitation. Opt Mater 31:678–684
31. Goldys EM, Drozdowicz-Tomsia K, Jinjun S, Dosev D, Kennedy IM, Yatsunenko S, Godlewski M (2006) Optical characterization of Eu-doped and undoped Gd_2O_3 nanoparticles synthesized by the hydrogen flame pyrolysis method. J Am Chem Soc 128:14498–14505
32. Cao R, Liu S, Xie L, Pan Y, Cao J, Liu Y (2008) Influence of different site symmetries of Eu^{3+} centers on the luminescence properties of Anderson-based compounds. Inorg Chim Acta 361:2013–2018
33. Jia W, Liu H, Felofilov SP, Meltzer R, Jiao J (2000) Spectroscopic study of Eu^{3+}-doped and Eu^{3+}, Y^{3+}-codoped SiO_2 sol–gel glasses. J Alloys Compd 311:11–15
34. Yi W, Langsheng L, Huiqun Z, Ruiqin D (2006) Anneal and concentration effect on PL properties of sol–gel derived Eu^{3+} doped SiO_2 glass. J Rare Earth 24:199–203
35. Liu T, Wang Y, Qin H, Bai X, Dong B, Sun L, Song H (2011) Gd_2O_3:Eu^{3+} mesoporous SiO_2 bifunctional core–shell composites: fluorescence label and drug release. Mater Res Bull 46:2296–2303
36. Song HW, Yu L, Lu S, Wang T, Liu Z, Yang L (2004) Remarkable differences in photoluminescent properties between LaPO4: Eu one-dimensional nanowires and zero-dimensional nanoparticles. Appl Phys Lett 85:470–472
37. Henderson B, Imbusch GF (1989) Optical spectroscopy of inorganic solids. Clarendon Press, Oxford, p 173
38. Boyd R (1992) Nonlinear optics. Academic Press, London, p 130
39. Shannon RD (1976) Revised effective ionic radii and systematic studies of interatomic distances in halides and chalcogenides. Acta Cryst A32:751–767

40. Vallet-Regí M, Manzano M, González-Calbet JM, Okunish E (2010) Evidence of drugs confinement into silica mesoporous matrices by STEM Cs corrected microscopy. Chem Commun 46:2956–2958
41. Almeida RM, Guiton TA, Pantano CG (1990) Characterization of silica gels by infrared reflection spectroscopy. J Non-cryst Solid 121:193–197
42. Almeida RM, Pantano CG (1990) Structural Investigation of silica gels films by infrared spectroscopy. J Appl Phys 58:4225–4232